Canadian Mineralogist
Vol. 16, pp. 175-186 (1978)

THE STRUCTURAL MORPHOLOGY OF OLIVINE. I. A QUALITATIVE DERIVATION

J. 'T HART
Geological and Mineralogical Institute, State University of Leiden, The Netherlands

Abstract

A qualitative derivation of the morphology of the olivine-type structure is given. To this end the *P*eriodic *B*ond *C*hains and *F* faces are derived from the orthorhombic structure according to the *PBC* theory of Hartman & Perdok. In this structure two types of bonds are present, the Mg–O bond and the much stronger Si–O bond. Within the *PBC*s the SiO_4 tetrahedra are considered complete crystallizing units; they are connected by the "weaker" Mg–O bonds. The *PBC* directions in order of increasing period are: [100], [001], <101>, [010], <201>, <110>, <111>, <210>, <211>, <012>, <112>, <310>, <212> and <311>. The *F* faces containing at least two *PBC*s within a growth layer d_{hkl} are: {010}, {110}, {021}, {101}, {111}, {120}, {121}, {001}, {130}, {112} and {132}. Projections of the structure parallel to *PBC*s with short periodicity show the relative order of importance of *F* faces within the zones parallel to the shortest *PBC*s. Thus we obtain, for the [001] zone: {010}, {110}, {120}, {130}; for the [100] zone: {010}, {021}, {001}; for the <101> zones: {010}, {101}, {111}, {121}; and for the <201> zones: {010}, {112}, {132}.

Sommaire

Pour établir qualitativement la morphologie de la structure cristalline du type olivine, on identifie les chaînes de liaison périodiques (*CLP*) et les faces *F* dans cette structure orthorhombique, suivant la théorie des *CLP* de Hartman & Perdok. Dans cette structure, on trouve deux types de liaison: type Mg–O et type Si–O; la liaison du type Si–O est de beaucoup la plus forte des deux. A l'intérieur des *CLP*, les tétraèdres SiO_4 sont considérés comme des éléments complets de cristallisation, reliés par les liaisons Mg–O. Les directions de *CLP* se rangent comme suit par ordre de période croissante: [100], [001], <101>, [010], <201>, <110>, <111>, <210>, <211>, <012>, <112>, <310>, <212> et <311>. Les faces *F* contenant au moins deux CLP dans l'épaisseur d'une couche de croissance d_{hkl} sont: {010}, {110}, {021}, {101}, {111}, {120}, {121}, {001}, {130}, {112} et {132}. Les projections de la structure parallèlement aux *CLP* de période courte montrent l'importance relative des faces *F* dans les zones parallèles à ces *CLP*. On obtient ainsi, pour la zone [001]: {010}, {110}, {120}, {130}; pour la zone [100]: {010}, {021}, {001}; pour les zones <101>: {010}, {101}, {111}, {121}; pour les zones <201>: {010}, {112}, {132}.

(Traduit par la Rédaction)

Introduction

Olivine crystals occur in many forms (Goldschmidt 1920) but are most commonly elongate along the *c* axis and flattened parallel to the (010) face. In naturally occurring crystals the most important forms are {010}, {110}, {021}, {111}, {120}, {101} and {001}, and the less important are {011}, {100}, {121} and {131}. Under special conditions, however, faces with higher indices may occur. The {112} form of olivine is commonly observed in meteorites only (Goldschmidt 1920).

The variation in morphology may be caused by many variables. These may be internal, such as distribution of dislocations and twin boundaries, or external, such as temperature, pressure, supersaturation, diffusion rate and presence of foreign materials. Before we can discuss the influence of each of these variables, we have to define a basic model. We assume that the morphology of a crystal is mainly determined by its structure and bond assemblage. As a consequence of this assumption the morphology of the Mg end member of the alivine series, forsterite (Mg_2SiO_4), can be derived from its structure. This is done here in a qualitative way by means of the *PBC* (Periodic Bond Chain) theory (Hartman & Perdok 1955a) and will be done in a quantitative way in a forthcoming paper (Part II). A qualitative derivation of *F* faces has already been given by Bautsch *et al.* (1971), but there a different criterion for choosing the *PBC*s was used, resulting in a different list of *PBC*s and *F* faces (see discussion).

Theoretical Background

According to the *PBC* theory (Hartman & Perdok 1955a; Hartman 1963, 1969, 1973) the habit of a crystal is determined by uninterrupted chains of strong bonds (*PBC*s). Strong bonds constituting a *PBC* are bonds in the first coordination sphere of an atom, ion or molecule which are formed during the crystallization process. The bond strength of Si–O and Mg–O (Brown & Shannon 1973) differs greatly in the first and

second coordination spheres as a function of the interatomic distances: Mg–O bonds of the second coordination sphere have a minimum length of 3.51Å, which results in a bond strength about ten times smaller than for the first coordination sphere (bond length 2.06-2.22Å); Si–O bonds have a much higher specific bond strength and therefore are used, as much as possible, in the formation of *PBC*s. The *PBC*s are chosen in such a way that only Mg–O bonds are broken.

Combinations of *PBC*s define three types of faces: A) *F* (flat) faces contain *PBC*s in at least two different directions and are formed by slices that grow slowly according to a layer mechanism. In agreement with current crystal-growth theories (Stranski 1928; Laudise 1970) it is assumed that the growth layers that contain the *PBC*s are slices having thicknesses d_{hkl}, determined by the cell dimensions and the space group. This implies that d_{hkl} is the repeat period of the minimum surface energy (Hartman 1973). B) *S* (stepped) faces have one *PBC* within the slice and grow faster than *F* faces. C) *K* (kinked) faces have no *PBC* within the slice and grow the fastest because there is no nucleation barrier.

The slow-growing *F* faces are the most important whereas the fast-growing *K* faces are unimportant and do not normally occur on the crystal. *S* faces have an intermediate position. In general, a crystal growing slowly from a slightly supersaturated vapor or solution and with sufficient *PBC*s in the structure, will be bounded exclusively by *F* faces. A face can grow in two ways; by means of two-dimensional nucleation for ideal crystals, and by means of a screw-dislocation mechanism for real crystals. A *PBC* should be given a stoichiometric composition because the growth process is considered as a consecutive formation of strong bonds. Furthermore, in ionic crystals with a centre of symmetry, a slice should not have a dipole moment perpendicular to its plane, because this would lead to crystal surfaces with a high electrostatic potential and consequently a high growth rate. As a consequence a *PBC* should not have a dipole moment perpendicular to its chain direction (Hartman 1973). For most faces, discrepancy between theoretical and observed morphology is mainly indicative of the influence of external factors, primarily solvent and impurity effects, but may also be due to the internal factors of twinning and dislocations.

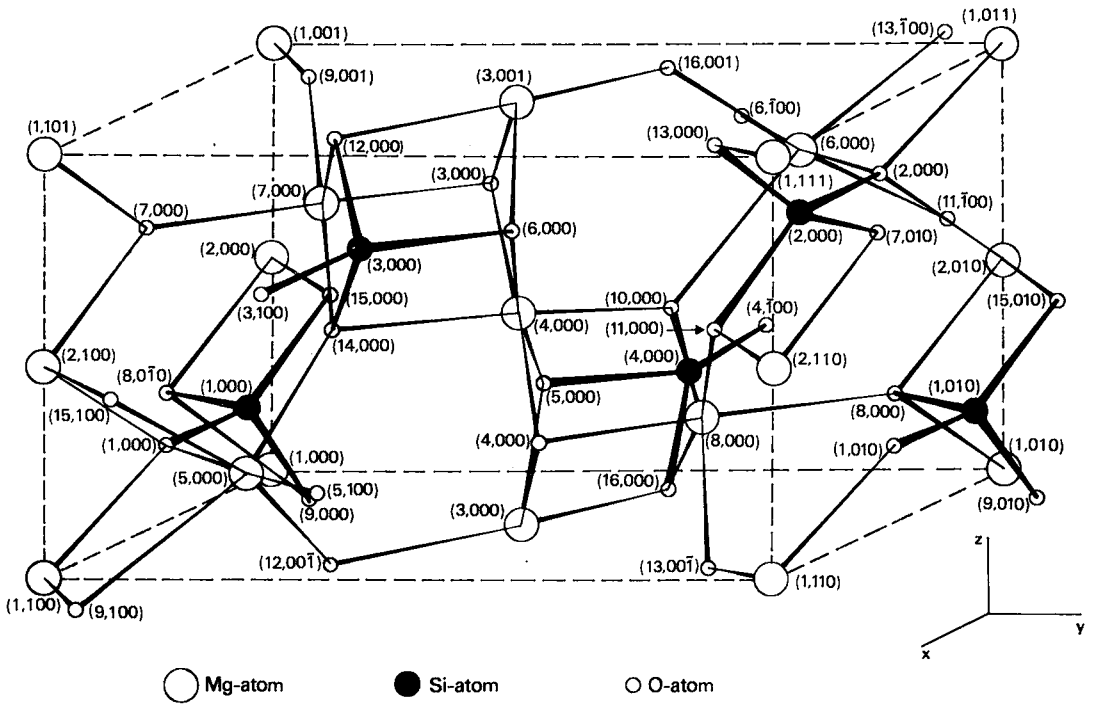

FIG. 1. The olivine unit cell. All atoms are numbered and are accompanied by translations in the *x*, *y* and *z* directions with respect to the chosen cell. Si–O bonds are heavily drawn. Other lines are Mg–O bonds.

The Crystal Structure

The orthorhombic structure of olivine was first determined on a forsteritic olivine, $(Mg,Fe)_2SiO_4$, by Bragg & Brown (1926). Later the structure was refined in space group *Pbnm* by Belov *et al.* (1951), Hanke & Zemann (1963), Hanke (1965) and finally by Birle *et al.* (1968). The structure consists of a nearly hexagonal close-packing of oxygen atoms parallel to the (100) plane (Fig. 1). One half of the octahedral sites are occupied by Mg(Fe) atoms, and one eighth of the tetrahedral sites by Si atoms. There are two different types of octahedral sites, *M*(I) on inversion centres, and *M*(II) on mirror planes. Serrate chains with a core of *M*(I) octahedra that share edges are connected with *M*(II) octahedra alternating left and right, and are parallel to the *c* axis. Those chains go through the origin and through (½,½, 0); they are connected with neighboring chains by SiO_4 tetrahedra and occupied *M*(II) octahedra. The rather high distortion, especially of the *M*(II) polyhedra, is an important feature. Each oxygen atom is bonded to one Si atom and three Mg atoms.

Derivation of *PBC*s and *F* Faces from the Structure

Derivation of *PBC*s and *F* Faces from the structure is based on cell and atomic parameters (Table 1) determined by Birle *et al.* (1968). All the bonds occurring within one unit cell and within the first coordination sphere, and the bond lengths between cations and anions (Birle *et al.* 1968) are given in Table 2. There are four formula units per cell, with four Mg atoms in *M*(I) positions, labeled 1 to 4, and four Mg atoms in *M*(II) positions, labeled 5 to 8.

TABLE 1. CELL AND ATOMIC PARAMETERS OF FORSTERITE*

a 4.762 Å	*b* 10.225 Å	*c* 5.994 Å	
Atom	*x*	*y*	*z*
M(I)	0	0	0
M(II)	0.98975(29)	0.27743(16)	¼
Si	0.42693(27)	0.09434(13)	¼
O(I)	0.76580(72)	0.09186(36)	¼
O(II)	0.22012(72)	0.44779(36)	¼
O(III)	0.27810(50)	0.16346(25)	0.03431(46)

* parameters of Birle *et al.* (1968)

The Si and O atoms also are labeled in this way (Fig. 1, Table 2). Where necessary, atoms have been translated in the direction [*uvw*] to neighboring unit cells. This translation is indicated after the index number of the atom. For instance, the oxygen atom O(1,$\bar{1}$00) has been translated by one period in the direction [$\bar{1}$00].

TABLE 2. CATION-ANION BONDS (Å) WITHIN THE FIRST COORDINATION SPHERE IN ONE UNIT CELL

	2.091(2)	2.091(2)	2.075(2)	2.075(2)	2.142(3)	2.142(3)
Mg(1)	O(1,$\bar{1}$00)	O(2,0$\bar{1}\bar{1}$)	O(7,$\bar{1}$0$\bar{1}$)	O(8,0$\bar{1}$0)	O(9)	O(13,$\bar{1}\bar{1}\bar{1}$)
Mg(2)	O(1,$\bar{1}$00)	O(2,0$\bar{1}$0)	O(7,$\bar{1}$00)	O(8,0$\bar{1}$0)	O(11,$\bar{1}\bar{1}$0)	O(15)
Mg(3)	O(3,00$\bar{1}$)	O(4)	O(5)	O(6,00$\bar{1}$)	O(12,00$\bar{1}$)	O(16)
Mg(4)	O(3)	O(4)	O(5)	O(6)	O(10)	O(14)
	2.177(4)	2.059(4)	2.217(3)	2.070(3)	2.070(3)	2.217(3)
Mg(5)	O(1)	O(5,100)	O(9,100)	O(12,00$\bar{1}$)	O(14)	O(15,100)
Mg(6)	O(2)	O(6,$\bar{1}$00)	O(11,$\bar{1}$00)	O(10)	O(16,001)	O(13,$\bar{1}$00)
Mg(7)	O(3)	O(7)	O(12)	O(9,001)	O(15)	O(14)
Mg(8)	O(4)	O(8)	O(10)	O(11)	O(13,00$\bar{1}$)	O(16)
	1.614(4)	1.635(3)	1.635(3)	1.654(4)		
Si(1)	O(1)	O(9)	O(15)	O(8,0$\bar{1}$0)		
Si(2)	O(2)	O(11)	O(13)	O(7,010)		
Si(3)	O(3,100)	O(12)	O(14)	O(6)		
Si(4)	O(4,$\bar{1}$00)	O(10)	O(16)	O(5)		

A slice d_{hkl} is an infinite layer of stoichiometric composition. Its thickness d_{hkl} is equal to the distance through which, for olivine, the surface energy remains constant. For some slices the thickness d_{hkl} is halved in accordance with the extinction conditions for the olivine-type structure, as determined by X-ray analysis.

We consider the structure of pure forsterite (Mg_2SiO_4). The SiO_4 tetrahedra are considered as complete crystallizing particles of the *PBC*, because the Si–O bonds are much stronger than the Mg–O bonds, and SiO_4 groups are present in the melt before crystals form. The crystallization process is therefore reduced to the formation of Mg–O bonds.

It is commonly possible to form more than one *PBC* per unit cell in a given direction [*uvw*]. For example, as there are four formula units per unit cell, there can exist two symmetry-related *PBC*s, each of which contains two formula units per period. In order to describe the *PBC*s for this relatively complicated structure, it is necessary to define a few terms. A *primitive PBC* (Woensdregt, pers. comm.) is defined as an uninterrupted periodic chain of strong bonds disregarding the condition of stoichiometry and electroneutrality. A *partial PBC* is defined as an uninterrupted chain of strong bonds, consisting of one or more primitive *PBC*s and additional ions so as to be electrostatically neutral. In the present case of olivine, this latter condition implies a stoichiometric composition because the SiO_4^{4-} tetrahedra are considered as complete crystallizing particles, so all anions have to be present. A *PBC* (or complete *PBC*) may consist of two or more partial *PBC*s. For

some directions it may occur that the addition of Mg ions to a primitive *PBC* transforms it directly into a complete *PBC* without the intermediate step of a partial *PBC*. The additional Mg ions (not being part of a primitive *PBC*) sometimes lie exactly on the boundary between two adjacent slices. In these cases they are statistically divided between these two slices.

In order to determine the *PBC*s, projections of the structure have been drawn parallel to all the directions of *PBC*s. This has been done using a Fortran IV program written for an IBM 370 computer connected with a Calcomp plotter (Woensdregt, pers. comm.). This method is followed because 1) in these projections it is easy to find out whether or not neighboring *PBC*s are bonded and 2) the surface structure of slices of different *F* faces can be seen and compared.

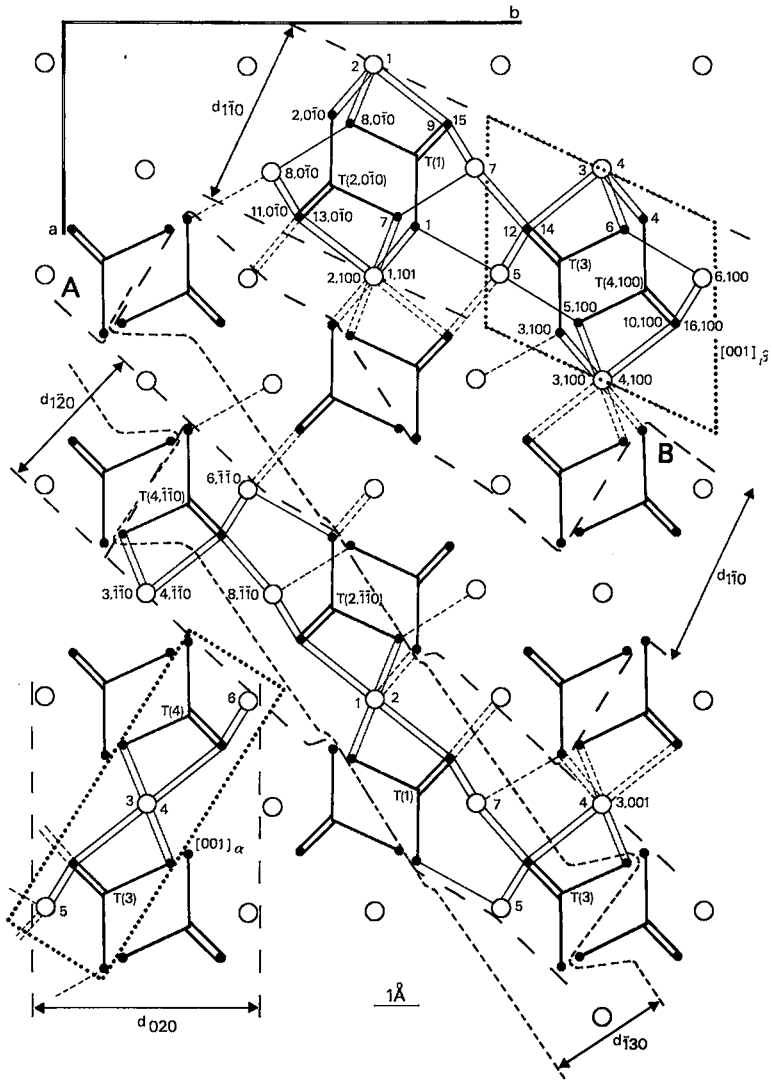

FIG. 2. Projection along [001], with slices d_{020}, $d_{1\bar{1}0}$, $d_{1\bar{2}0}$ and $d_{1\bar{3}0}$. Black dots are oxygen atoms, open circles magnesium atoms and heavy lines represent the SiO_4 tetrahedra with the silicon atom in the centre. In the case of two numbers accompanying one symbol, two atoms of the same type lie one above the other. The dangling bonds on the surface of the slices are dashed.

THE [001] ZONE

The projection along [001] is drawn in Figure 2. In this direction there exists a primitive *PBC*: $T(4)$–Mg(6)–$T(4,001)$, where $T(4)$ represents the SiO_4 tetrahedron around Si(4), including the four surrounding oxygen atoms. There are four such primitive *PBC*s per unit cell. They have to be combined with the remaining Mg ions to form partial *PBC*s and these must be combined to form complete *PBC*s which should be centrosymmetric (no dipole moment perpendicular to [001]). This latter combination can be done only by using either the centres of symmetry in the structure (there are two, one occupied by a M(I) ion, the other empty), or by the two-fold screw axis. Two different *PBC*s are theoretically possible, $[001]_\alpha$ and $[001]_\beta$. The first, $[001]_\alpha$, is a combination of two primitive *PBC*s by the symmetry centre at an M(I) site. This *PBC* is outlined in Figure 2 in the slice d_{020}. One primitive *PBC* contains $T(4)$ and Mg(6), the other $T(3)$ and Mg(5), whereas Mg(3) and Mg(4) serve two purposes: to transform the primitive *PBC*s into partial *PBC*s and to connect the partials to one complete *PBC*. The second, $[001]_\beta$, is shown in Figure 2 in the slice $d_{1\bar{1}0}$. A primitive *PBC* containing $T(3)$ and Mg(5) is combined *via* a centre of symmetry with the primitive *PBC* combining $T(4,100)$ and Mg(6,100). The former primitive *PBC* is transformed into a partial one by adding ½Mg(3) and ½Mg(4). Similarly, ½Mg(3,100) and ½Mg(4,100) are added to the other primitive *PBC*. The ions are taken for half of their charge because they lie one above the other in the direction [001] and there is no preference at this stage. These *PBC*s are connected to surrounding *PBC*s in the following slices.

The $d_{\bar{1}20}$ slice

This slice can be considered to consist of a row of parallel *PBC*s $[001]_\alpha$ as well as $[001]_\beta$. In both cases the surface structure of the slice (Fig. 2) is the same. Within the slice the *PBC*s are connected in the [100], <101> and <201> directions, so new *PBC*s lie parallel to these directions.

The $d_{1\bar{2}0}$ slice

Here *PBC*s $[001]_\alpha$ and $[001]_\beta$ alternate. The former has its centres of symmetry in Mg(1) and Mg(2), whereas for the latter the centre is between $T(3)$ and $T(4,100)$. The $[001]_\beta$ *PBC* has been symmetrically divided on both sides of the $[001]_\alpha$ *PBC* in Figure 2, because when defined this way the *PBC* can be used also for the $d_{1\bar{1}0}$ slice.

Note that the boundary between two consecutive slices cannot be represented by a mathematical plane, because the "tops" of the two SiO_4 tetrahedra are situated partly outside that plane. This gives the surface of $(1\bar{2}0)$ an undulated structure. The Mg(3 and 4) ions have to be divided statistically between neighboring slices. Within the $d_{1\bar{2}0}$ slice the *PBC*s are bonded in the [210], [211], [212], $[21\bar{1}]$ and $[21\bar{2}]$ directions.

The $d_{1\bar{1}0}$ slice

Slices can be formed in two ways. First, in the upper right portion of Figure 2 a slice is shown in which two $[001]_\beta$ *PBC*s, related to each other by the glide plane n parallel to (010), alternate. The M(I) octahedra are all situated at the boundary of the slice and have to be divided between the neighboring slices. The $[001]_\beta$ *PBC*s are bonded together in the direction [110], [111], $[11\bar{1}]$, [112] and $[11\bar{2}]$.

The second possibility is to combine two $[001]_\alpha$ *PBC*s, again related by the glide plane n, as indicated in Figure 2, between the former $d_{1\bar{1}0}$ slice and the $d_{1\bar{2}0}$ slice. The surface of this slice is highly undulating as shown by the line AB, but has no M(I) positions on its boundary. The $[001]_\alpha$ *PBC*s are bonded together in the same directions as the $[001]_\beta$ *PBC*s. Which of the two surfaces is the more stable cannot be decided at this stage; this has to be evaluated on the basis of surface energy considerations (Part II).

The $d_{1\bar{3}0}$ slice

The $d_{1\bar{3}0}$ slice is defined by nearly the same complete *PBC* as outlined within the $d_{1\bar{2}0}$ slice. Only Mg(3,$\bar{1}\bar{1}$0) and Mg(4,$\bar{1}\bar{1}$0) are replaced by Mg(3,$\bar{2}\bar{1}$0) and Mg(4,$\bar{2}\bar{1}$0); Mg(3,001) and Mg(4) are replaced by Mg(3,101) and Mg(4,100). Translation of these *PBC*s in the [310], $[31\bar{1}]$ and [311] directions define the $d_{1\bar{3}0}$ slice.

The forms {020}, {120}, {110} and {130} are all F forms because there are within each slice at least two *PBC*s in different directions. A fifth slice d_{200} contains only *PBC*s parallel to the [001] direction, so the {100} form is an S face. Theoretically, this diminishes the chance that this form will be present on a crystal.

THE [100] ZONE

A primitive *PBC* [100] can be constituted in three ways (Fig. 3): $T(1)$–Mg(5)–$T(1,100)$, $T(1)$–$Mg(1)$–$T(1,100)$ or $T(1)$–$Mg(2)$–$T(1,100)$. There are always four such primitive *PBC*s per unit cell, whatever type is chosen. The partial *PBC*s

are obtained by adding the missing Mg ions. For the first primitive *PBC* this must be either Mg(1) or Mg (2) or ½Mg(1) + ½Mg(2). For the second and third primitive *PBC* this can be one of Mg(5), Mg(7), Mg(7,00$\bar{1}$) or Mg(8,0$\bar{1}$0). Combination of the partial *PBC*s leads to the following slices.

The d_{020} slice

Here the partial *PBC*s are connected by the inversion centres in the *M*(I) sites. For example *T*(1) and *T*(2,0$\bar{1}$0) are connected by Mg(2). Now two surfaces are possible: firstly, the surface already obtained in the [001] projection, by addition of Mg(7) and Mg(8,0$\bar{1}$0); secondly, an undulating surface, by addition of Mg(5) and Mg(6,0$\bar{1}$0). Energy considerations are necessary to find the more favorable surface.

The d_{021} slice

In this slice two partial *PBC*s are connected by Mg(2), the other two by Mg(4,00$\bar{1}$) (Fig. 3). The complete *PBC*s can be formed in two ways. One *PBC* comprises *T*(1), *T*(2,0$\bar{1}$0), Mg(2), ½Mg(1) and ½Mg(1,101), together with Mg(5,$\bar{1}$00) and Mg(6,1$\bar{1}$0). Through the action of the glide plane *b* parallel to (100) and a translation of [00$\bar{1}$] we find the equivalent *PBC* centred around Mg(4,00$\bar{1}$). This sequence of *PBC*s gives a d_{021} slice with a planar boundary. Another PBC is obtained if instead of Mg(5,$\bar{1}$00) and Mg(6,1$\bar{1}$0), Mg(8,0$\bar{1}$0) and Mg(7) are used. However, this *PBC* is not bonded to its neighbors. Within the slice drawn in Figure 3, the *PBC*s are bonded in the directions [0$\bar{1}$2], [1$\bar{1}$2], [$\bar{1}\bar{1}$2], [2$\bar{1}$2], and [$\bar{2}\bar{1}$2]. The <012> are new *PBC* directions.

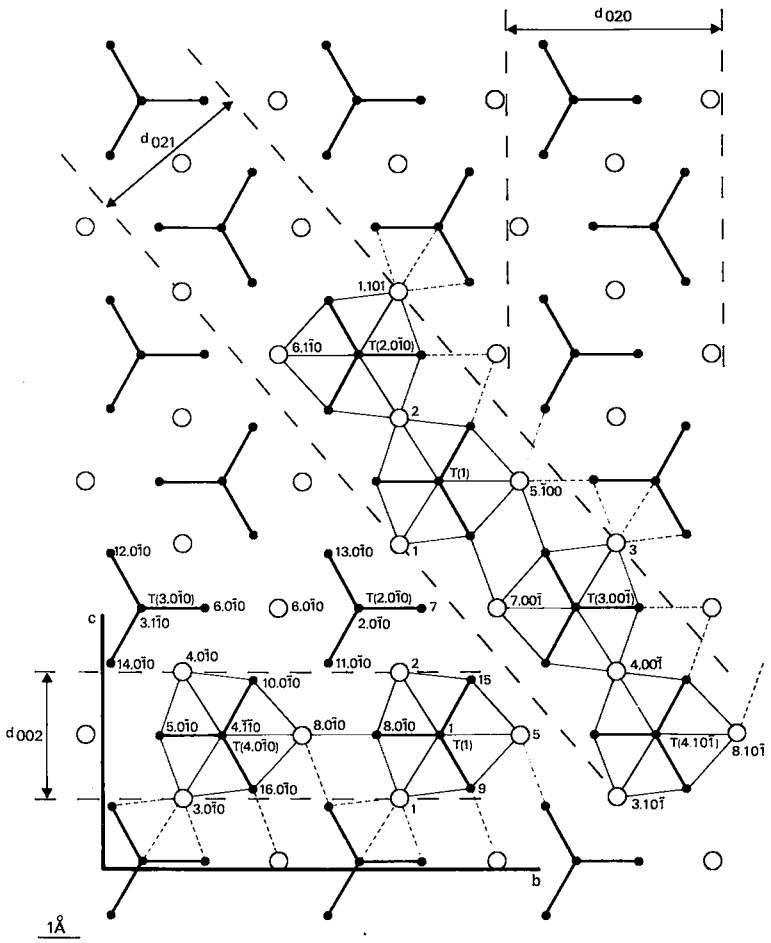

FIG. 3. Projection along [100], with the slices d_{020}, d_{021} and d_{002}. Symbols as in Figure 2.

The d_{022} slice

As $k=2n$ for $0kl$, the d_{011} value should be halved to d_{022}. This slice only contains *PBC*s [100] that are not bonded to their neighbors, so {011} is an *S* form.

The d_{002} slice

This slice (Fig. 3) consists of a series of parallel [100] partial *PBC*s through the action of the glide plane *b* parallel to (100). One such partial *PBC* consists of *T*(1), Mg(5), ½Mg(1) and ½Mg(2). Although each of these partial *PBC*s has a dipole moment perpendicular to its direction [100], the slice d_{002} has not, because of the symmetry plane parallel to (001). The *PBC*s are bonded in the directions [110], [1$\bar{1}$0] and [010], which introduces the new *PBC* [010].

The [101] Zone

In the [001] projection (Fig. 2), it was shown that the *PBC*s in the d_{020} slice were also bonded in the [101] direction. A projection parallel to this direction (Fig. 4) shows the slices $d_{10\bar{1}}$, $d_{11\bar{1}}$ and $d_{\bar{1}21}$. It is possible to form two different *PBC*s, $[101]_\alpha$ and $[101]_\beta$. The $[101]_\alpha$ *PBC* is based on the primitive *PBC* Mg(1)–T(1)–[Mg(7)

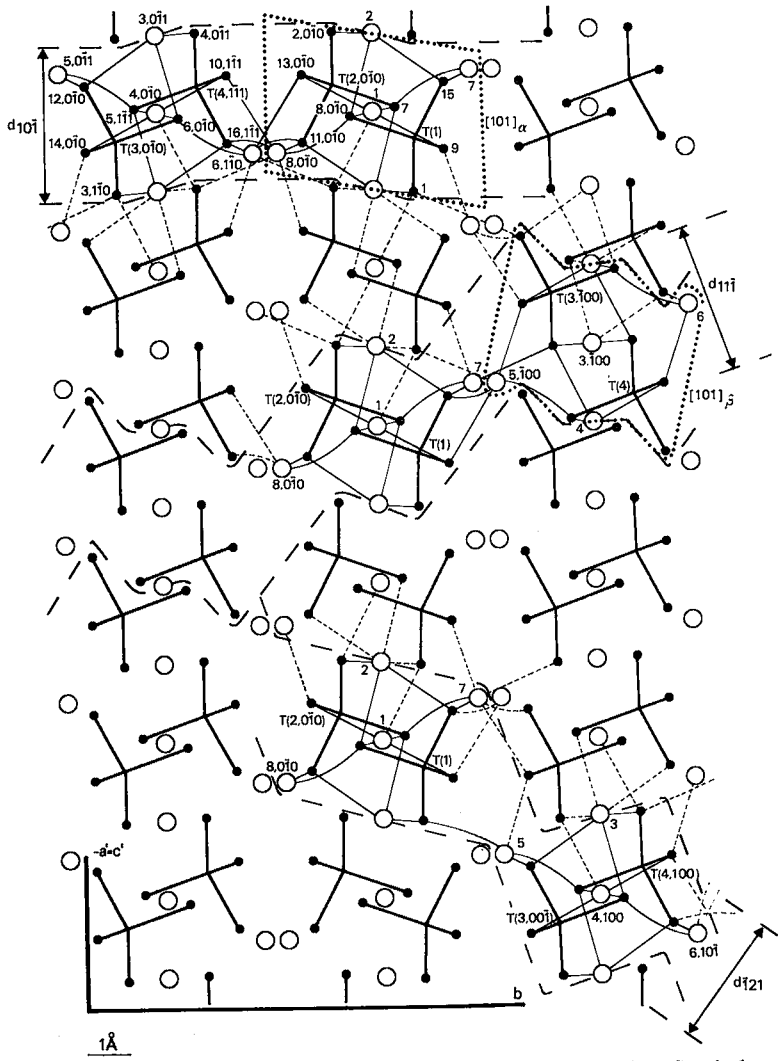

FIG. 4. Projection along [101], with the slices $d_{10\bar{1}}$, $d_{11\bar{1}}$ and $d_{\bar{1}21}$. Symbols as in Figure 2.

or Mg(8,0$\bar{1}$0)]–T(2,0$\bar{1}$0)–Mg(1,101). The addition of ½Mg(2) and ½Mg(2,100) suffices to transform it into a complete *PBC*, shown in the upper part of Figure 4.

The $[101]_\beta$ *PBC* contains the primitive *PBC* Mg(3,$\bar{1}$00)–T(4)–[Mg(6) or Mg(5,100)]-T(3,$\bar{1}$00)–Mg(3,001). Here a complete *PBC* is obtained by the addition of ½Mg(4) and ½Mg(4,$\bar{1}$00).

To each of the described *PBC*s belongs a symmetrically equivalent *PBC* within the unit cell. The $[101]_\alpha$ have their symmetry centre in Mg(1) or Mg(4), the $[101]_\beta$ in Mg(2) or Mg(3).

The $d_{10\bar{1}}$ slice

A slice can be outlined which contains a combination of two equivalent $[101]_\alpha$ *PBCs* (Fig. 4). The surface is nearly flat with two M(I) octahedra at the slice boundary and the "tops" of the SiO_4 tetrahedra a bit outside the slice. The *PBC*s are bonded within the $d_{10\bar{1}}$ slice in the directions [010], [111] and [1$\bar{1}$1]. It is also possible to outline the $d_{10\bar{1}}$ slice by combination of two $[101]_\beta$ *PBC*s; this gives a far more undulating surface and is not represented in the figure.

The $d_{11\bar{1}}$ slice

The slice shown in the upper half of Figure 4 contains an alternating series of $[101]_\alpha$ and $[101]_\beta$ *PBC*s. In Figure 4 a combination has been made of the $[101]_\alpha$ with symmetry centre in Mg(1) and the $[101]_\beta$ with symmetry in Mg(3,$\bar{1}$00). It is also possible to translate the slice a distance ½$d_{11\bar{1}}$, so that instead of the $[101]_{\alpha+\beta}$, $[101]_{\beta+\alpha}$ is formed. This configuration of the slice is not represented in Figure 4, because from qualitative considerations it is not clear which is the most stable. Within the slice as represented in Figure 4, the *PBC*s are bonded in the [1$\bar{1}$0] direction. The SiO_4 tetrahedra produce a highly undulating surface on the slice. The O(16) and O(12) atoms are in especially unfavorable positions.

The $d_{\bar{1}21}$ slice

The same two equivalent *PBC*s used in the $d_{10\bar{1}}$ slice are used to delineate the $d_{\bar{1}21}$ slice, but they are bonded in different directions. Other chains of strong bonds within the $d_{\bar{1}21}$ slice lie parallel to the directions [11$\bar{1}$], [210] and [012].

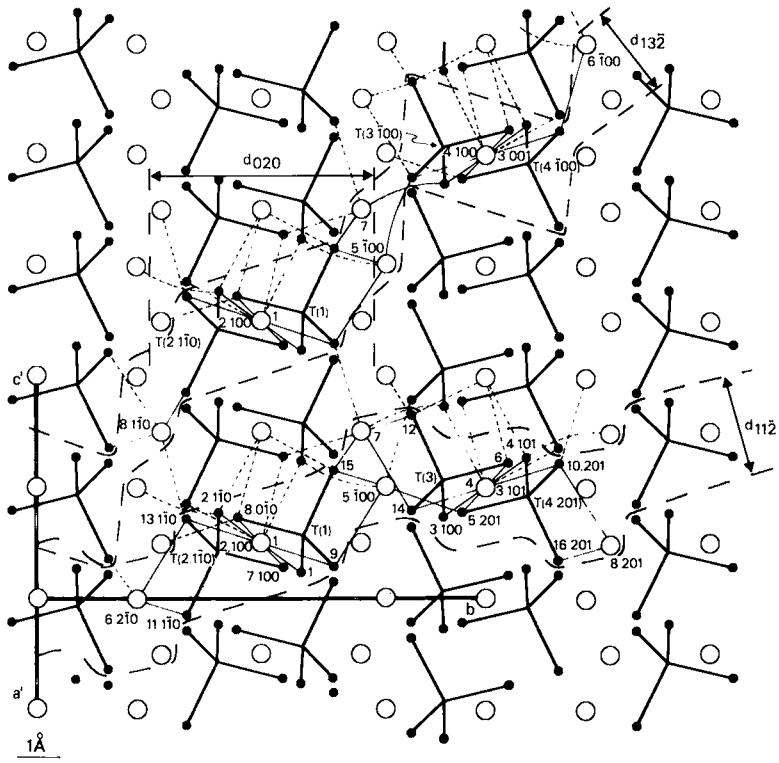

FIG. 5. Projection along [201], with the slices $d_{11\bar{2}}$ and $d_{13\bar{2}}$. Symbols as in Figure 2.

The [201] Zone

The primitive *PBC* (Fig. 5) can be described by: Mg(1)–*T*(1)–Mg(2,100)–*T*(2,1$\bar{1}$0)–Mg(1,201). Because the Mg ions in this chain lie at symmetry centers, the addition of Mg ions in the *M*(II) sites transforms this primitive *PBC* into a complete *PBC*. This can be done in various ways, namely by adding either Mg(5,$\bar{1}$00) and Mg(6,2$\bar{1}$0), or one of the following pairs: Mg(5) and Mg(6,110), Mg(7,001) and Mg(8,111), Mg(7) and Mg(8,1$\bar{1}$0), Mg(7,100) and Mg(8,0$\bar{1}$0). Equivalent *PBC*s are centred around Mg(4) and Mg(3,101) ions.

The d_{020} slice

The various *PBC*s give exactly the same two slices as are found before.

The $d_{11\bar{2}}$ slice

Figure 5 shows this slice, in which *PBC*s centred around Mg(1) and Mg(4) alternate. This slice has the energetically most favorable configuration (Part II) if the primitive *PBC* centred around Mg(2,100) is completed by Mg(5,$\bar{1}$00) and Mg(6,2$\bar{1}$0), and the primitive *PBC* centred around Mg(3,101) by Mg(7) and Mg(8,201) (Fig. 5). Within the slice there are also chains of strong bonds in the [1$\bar{1}$0] and [111] directions.

The $d_{13\bar{2}}$ slice

If we take the primitive *PBC* centred around Mg(3,001), completed with Mg(5,$\bar{1}$00) and Mg(6,$\bar{1}$00), and the primitive *PBC* centred around Mg(2,100) completed by Mg(7) and Mg(8,1$\bar{1}$0), then we can outline the $d_{13\bar{2}}$ slice (Fig. 5). Other directions parallel to chains of strong bonds within this slice are [310], [112] and [$\bar{1}$11].

Discussion

Only four projections parallel to the determined *PBC*s are shown (Figs. 2-5). These four *PBC*s have short periods (Table 3), so the drawing of one *PBC* in a projection is rather simple, because the bonds are clearly visible. However, for *PBC*s with long periods the drawing of all bonds results in a crowded figure, although the repeat pattern of identical *PBC*s is clear. Projections of the structure have also been made parallel to the other *PBC* directions (Table 3) but because they provide no extra information they are not presented here. As the *PBC* length increases, the strength generally decreases, so the projections in Figures 2 to 5 are parallel to the strongest *PBC*s.

TABLE 3. *PBC*s IN ORDER OF INCREASING LENGTH AND *F* FACES IN ORDER OF DECREASING d_{hkl} VALUES

*PBC**	Period	*F* form {*hkl*}	d_{hkl}
100	4.762	020	5.113
001	5.994	110	4.317
101	7.655	021	3.890
010	10.225	101	3.729
201	11.253	111	3.503
110	11.280	120	3.485
111	12.773	121	3.013
210	13.973	002	2.997
211	15.205	130	2.772
012	15.762	112	2.462
112	16.460	132	2.035
310	17.568		
212	18.411		
311	18.563		

* written as vector [*uvw*]; period and d_{hkl} in Å

The zones parallel to *PBC*s and the *F* faces have been drawn in a stereographic projection (Fig. 6). Not all points of intersection of zones parallel to *PBC*s will produce an *F* face; if the thickness d_{hkl} of the corresponding growth slice is too small to contain *PBC*s in one or more directions, the point of intersection produces an *S* face (d_{022} and d_{200}) or *K* face.

The faces are presented in Table 3 in order

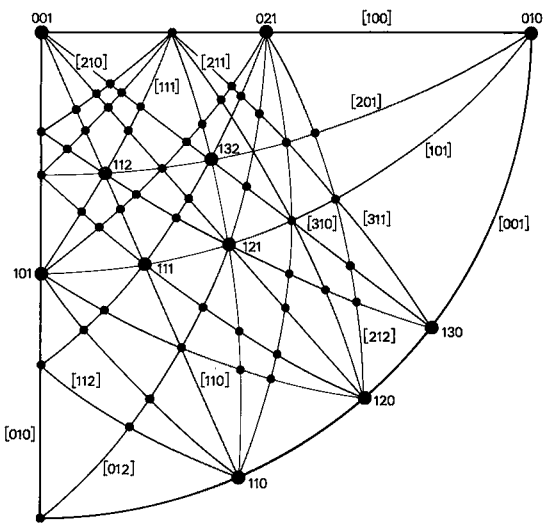

FIG. 6. One fourth of a stereographic projection with the zones parallel to the *PBC* directions which occur on the upper hemisphere. Big dots at the intersection of two or more zones are *F* faces. The small dots represent *S* and *K* faces.

of decreasing d_{hkl} values, according to the law of Bravais-Friedel (Friedel 1907) as extended by Donnay & Harker (1937). According to this law, the {020} form should be the most important one. Considering Figure 6, we see that there are four short (*i.e.*, strong) *PBC*s in the [001], [100], <101> and <201> directions within the d_{020} slice. The suggestion that {010} is the most important form has already been made by many authors (*e.g.*, Laspeyres 1883, Zambonini 1905, Soūza-Brandão 1911, Fleet 1975). Sobolev *et al.* (1970) observed olivine crystals in diamond with {010} as the most important form; that these are also elongate parallel to [001] is predictable because the strongest *PBC*, the one with most Mg–O bonds between the SiO_4 tetrahedra, is parallel to the [001] direction.

The occurrence of the {110} and {120} forms in the [001] zone merits some discussion. The d_{110} slice can be formed by two different *PBC*s, either by the two equivalent $[001]_\beta$ *PBC*s as shown within the $d_{1\bar{1}0}$ slice, or by the two equivalent $[001]_\alpha$ *PBC*s (Fig. 2). For the former case all the Mg atoms in *M*(I) positions have to be divided statistically in the neighboring slices, which is energetically unfavorable (Part II). In the latter case a highly undulating slice surface is formed, which also seems energetically unfavorable. It is not, therefore, qualitatively possible to decide which *PBC* will give the best results for the d_{110} slice.

If we consider in Figure 2 the $d_{1\bar{2}0}$ slice and the $d_{1\bar{1}0}$ slice in the middle of the drawing, it can be seen that they have in common the *PBC* $[001]_\alpha$ and two halves of the *PBC* $[001]_\beta$ on either side. In the slice $d_{1\bar{2}0}$ this common part can be recognized as the part where all Si–O and Mg–O bonds are drawn. The difference between the $d_{1\bar{1}0}$ and $d_{1\bar{2}0}$ slices then lies in the way these common parts are bonded together. It seems then that the *PBC*s are more strongly bonded within the $d_{1\bar{1}0}$ slice, which moreover has a higher d_{hkl} value. Therefore, one could expect {110} to be more important than {120}. Within the d_{130} slice the neighboring *PBC*s are only bonded by two Mg–O bonds, which makes this slice again less important than d_{120}.

In the [100] zone the order of importance of the slices is $d_{020} > d_{021} > d_{002}$. The last one is far from ideal because all the *M*(I) positions are situated on the slice boundary. The d_{020} slice is more important than the d_{021} because it has the highest d_{hkl} value, the shortest *PBC*s within the slice, and no *M*(I) positions on the slice boundary. This agrees well with observations of crystals in nature. Artificial cobalt olivine shows the same succession of faces in this zone ('t Hart & Wessicken 1977), just as the forsterite grown by Vu Tien *et al.* (1972).

Of the different *F* faces in the <101> zones, the {101} form is probably more important than {111} and {121}. Within the $d_{10\bar{1}}$ slice the two equivalent $[101]_\alpha$ *PBC*s are bonded by four Mg–O bonds per period, and within the $d_{\bar{1}21}$ slice only by one (Fig. 4). The d_{101} slice has a higher d_{hkl} value than the d_{121} slice and within the d_{101} slice there are *PBC*s with shorter periods (Fig. 6).

If we compare the {111} and {121} forms, we notice that the $d_{11\bar{1}}$ slice is composed of a $[101]_\alpha$ and $[101]_\beta$ *PBC*, whereas the $d_{\bar{1}21}$ slice consists of two $[101]_\alpha$ *PBC*s. Within the $d_{11\bar{1}}$ slice the *PBC*s are bonded by three Mg–O bonds and within the $d_{\bar{1}21}$ slice only by one. Based on these considerations, one may expect that the {111} form is more important than the {121} form. The last *F* faces, {112} and {132} are clearly shown in the [201] projection. In nature these are the least observed *F* forms, with the lowest d_{hkl} values. If we compare the {112} form with the {111} and {121} forms, we observe that in the d_{112} slice all the cations are situated rather close to the centre of the slice, which influences the energy values favorably (Part II). But, because the slice is so narrow, it has one of the highest numbers of dangling bonds of all the *F* faces. So it is clearly difficult to make a comparison between the {112} form and the other two bipyramidal forms on the basis of qualitative considerations only. Presumably the {112} form is more important than the {132} form, because within the d_{112} slice the *PBC*s are slightly more strongly bonded to their neighbors.

It is possible to predict, from the structure, which crystal faces are most susceptible to impurity and supersaturation effects. For these effects we have to look at the distribution of cations and anions within the slices. From Figure 2 it can be seen that layers of negatively charged oxygen ions in a hexagonal close-packing alternate with layers of positive ions (Si^{4+} and Mg^{2+}). It has been shown (Kern 1953, 1955) that faces where positive and negative layers alternate (such as (111) of NaCl or (001) of CsCl) are good candidates for supersaturation and impurity effects. These faces have a high electrostatic potential on the surface, because the outermost layer contains ions of one kind only. As a consequence, dipole molecules like water and other particles are strongly absorbed at high supersaturation and this absorption may become a rate-determining factor.

The surface of the d_{020} slice consists of the

slightly larger M(II) octahedral positions, which may be occupied by bigger cations like Ca^{2+} (Fleet 1975). This may be a rate-determining factor for the growth velocity in the [010] direction.

Bautsch *et al.* (1971) derived *PBC*s and *F* faces from the structure to explain the presence of cleavage planes, but the criterion used for choosing the *PBC*s was different. They only looked for directions in which it was possible to form a chain of strong bonds between symmetry-related atoms (Hartman & Perdok 1955b), and not between translation-related atoms. However, the method of Hartman & Perdok (1955b) has been abandoned, because the symmetry at the surface differs from that in the bulk crystal. This is why a different list of *PBC*s and *F* faces is obtained here (Table 4). The cation–cation distance was used by Bautsch *et al.* as a criterion of strong bonding. In the present paper the criterion is the presence of at least one Mg–O bond between the SiO_4 tetrahedra in the direction parallel to the *PBC*.

Comparing the relative importance of crystal forms of Mg-rich olivine as proposed by Fleet (1975) with the results of the present work, it is found that the agreement between observed and derived morphology is satisfactory. This is due to the fact that in both papers SiO_4 tetrahedra are considered as complete crystallizing particles and the Mg–O bonds are considered the only bonds formed during the crystallization process. However, there are a few differences. Dipyramidal forms are not discussed by Fleet. Although they are not observed on skeletal crystals, they are commonly observed on polyhedral crystals. Growth layers, as indicated by Fleet (1975), have a high dipole moment, because for {021}, {110}, {120} (erroneously indexed as {210} throughout Fleet's paper), {101} and {001} all the M(I) and for {010} all the M(II) atoms are at one side of the growth layer. These atoms have to be divided statistically between two growth layers; otherwise, a tremendously high surface charge would occur. Taking into account this statistical division of the M(I) and M(II) atoms at the (010) surface, as given in Figure 2, the surface structures, as given intuitively by Fleet, have been given their foundation in the present paper.

TABLE 4. COMPARISON IN DERIVATION OF *PBC*s AND *F* FACES FROM THE STRUCTURE

Bautsch† *PBC**	this study *PBC**	face	face type Bautsch	face type this study
100	100	010	*F*	*F*
00½	001	110	*F*	*F*
101	101	021	*F*	*F*
-	010	101	*F*	*F*
10½	201	111	*F*	*F*
½½0	110	120	*S*	*F*
½½½	111	121	-	*F*
-	210	001	*F*	*F*
-	211	130	-	*F*
-	012	112	*F*	*F*
-	310	100	*S*	*S*
½½1	112	011	*F*	*S*
-	212	132	-	*F*
-	311			

† Bautsch *et al.* (1971); * written as a vector [*uvw*]

Fleet recognized correctly {100} as a stepped face, but this has nothing to do with the growth of {010}, because growth fronts parallel to [001] must be considered to be parts of {110} and {120} rather than of {100}. This phenomenon has been proved by observations on natural crystals; those that are flattened parallel to {100} show macro-steps parallel to {110} and {120}.

Conclusions

1. The *PBC*s in the olivine-type structure are: [100], [001], <101>, [010], <201>, <110>, <111>, <210>, <211>, <012>, <112>, <310>, <212> and <311>, if the SiO_4 tetrahedra are considered as complete crystallizing particles.
2. The *F* forms are: {010}, {110}, {021}, {101}, {111}, {120}, {121}, {001}, {130}, {112} and {132}.
3. The order of relative importance of the *F* faces in the zones parallel to *PBC*s, based on the bonds between these *PBC*s within the slices in this zone, is: for the [001] zone, {010}, {110}, {120} and {130}; for the [100] zone, {010}, {021} and {001}; for the <101> zones, {010}, {101}, {111} and {121}; for the <201> zones, {010}, {112} and {132}.
4. The *F* faces, derived from the structure, all belong to the most frequently observed crystal forms in nature, with the exception of the {112} and {132} forms. The {112} form is, according to the drawings of Goldschmidt's *Atlas der Krystallformen,* only frequently observed on olivine crystals from palasitic meteorites.
5. In contrast to Bautsch *et al.* (1971), we conclude that {120} is an *F* face and not an *S* face, {011} is an *S* face and not an *F* face, and {121}, {130} and {132} are *F* faces.
6. There is a significant difference between the growth layers (slices) as represented by Fleet (1975) and those presented in this paper. In the

growth layers illustrated by Fleet, the Mg atoms that are close to the boundary of the slice are presented only on one side of the boundary. This choice produces polarity, which should be avoided. A boundary should be chosen in such a way that there is a statistical distribution of Mg atoms at both sides of the slice boundary.
7. The derivation of the *F* faces in this paper provides the basis for a further quantitative derivation of the morphology of crystals with the olivine-type structure in Part II.

Acknowledgements

I am greatly indebted to Professor P. Hartman for advising me on the subject of this investigation, for his many stimulating discussions and for his critical reading of the manuscript. I am thankful especially to Drs. C. F. Woensdregt for his critical reading of the manuscript and his help in introducing me to the computer programmes. I further wish to thank Dr. P. Bennema for his valuable comments and criticism and Dr. C. S. Strom for correcting the English manuscript.

References

Bautsch, H. J., Fanter, D. & Melle, G. (1971): Kristalstructurelle Ableitung der Spaltbarkeit beim Olivin. *Ber. deut. Ges. geol. Wiss. B. Miner. Lagerstättenf.* **16**, 205-211.

Belov, N. V., Belova, E. N., Andrianova, N. H. & Smirnova, P. F. (1951): Determination of the parameters in the olivine (forsterite) structure with the harmonic three dimension synthesis. *Dokl. Akad. Nauk S.S.S.R.* **81**, 399-402.

Birle, J. D., Gibbs, G. V., Moore, P. B. & Smith, J. V. (1968): Crystal structures of natural olivines. *Amer. Mineral.* **53**, 807-824.

Bragg, W. L. & Brown, G. B. (1926): Die Struktur des Olivins. *Z. Krist.* **63**, 538-556.

Brown, I. D. & Shannon, R. D. (1973): Empirical bond-strength – bond-length curves for oxides. *Acta Cryst.* A**29**, 266-282.

Donnay, J. D. H. & Harker, D. (1937): A new law of crystal morphology extending the law of Bravais. *Amer. Mineral.* **22**, 446-467.

Fleet, M. E. (1975): The growth habits of olivine. A structural interpretation. *Can. Mineral.* **13**, 293-297.

Friedel, G. (1907): Etudes sur la loi de Bravais. *Bull. Soc. franç. Minéral.* **30**, 326-455.

Goldschmidt, V. (1920): *Atlas der Krystallformen.* **6**. Carl Winters Universitätsbuchhandlung, Heidelberg.

Hanke, K. (1965): Beiträge zu Kristallstrukturen vom Olivin-Typ. *Beitr. Mineral. Petrog.* **11**, 535-558.

——— & Zemann, J. (1963): Verfeinerung der Kristallstruktur von Olivin. *Naturwiss.* **50**, 91-92.

't Hart, J. & Wessicken, R. (1977): The morphology of cobalt-olivine (Co_2SiO_4). *Neues Jahrb. Mineral. Monatsh.*, 408-413.

Hartman, P. (1963): Structure, growth and morphology of crystals. *Z. Krist.* **119**, 65-78.

——— (1969): The dependence of crystal morphology on crystal structure. *In* Growth of Crystals 7 (N. N. Sheftal, ed.) Consultants Bureau, New York.

——— (1973): Structure and morphology. *In* Crystal Growth. An Introduction (P. Hartman ed.), North-Holland, Amsterdam.

——— & Perdok, W. G. (1955a): On the relations between structure and morphology of crystals I. *Acta Cryst.* **8**, 49-52.

——— & ——— (1955b): On the relations between structure and morphology of crystals III. *Acta Cryst.* **8**, 525-529.

Kern, R. (1953): Etude du faciès de quelques cristaux ioniques à structure simple. *Bull. Soc. franç. Minéral. Crist.* **76**, 325-364.

——— (1955): Influence du milieu de croissance sur la correspondance entre morphologie et structure cristalline. *Bull. Soc. franç. Minéral. Crist.* **78**, 461-474, 497-520.

Laspeyres, H. (1883): Künstliche Krystalle von Mangan-Eisen-Olivin. *Z. Krist. Mineral.* **7**, 494-498.

Laudise, R. A. (1970): *The Growth of Single Crystals.* Prentice-Hall, Englewood Cliffs, N.J.

Sobolev, N. V., Bastoshinskiy, Z. V., Yefimova, E. S., Lavrent'yev, Yu. G. & Pospelova, L. N. (1970): Olivine-garnet-chrome diopside assemblage from Yakutian diamond. *Dokl. Akad. Nauk S.S.S.R.* **192**, 134-137.

Souza-Brandão, V. (1911): Die Espichellite, eine neue Familie von Ganggesteinen am Vorgebirge Espichel. *Z. Krist. Mineral.* **49**, 292-293.

Stranski, I. N. (1928): Zur Theorie des Kristallwachstums. *Z. phys. Chem.* **136**, 259-278.

Vu Tien, L., Grandin de l'Eprevier, A., Gabis, V. & Anthony, A. M. (1972): Amélioration de la méthode des flux, synthèse et purification d'un minéral: la forstérite. *J. Crystal Growth*, 13/14, 601-603.

Woensdregt, C. F. (1970): CRYPRO. A Fortran IV program for making crystal structure projections. *Geol. Mineral. Inst. Leiden State Univ.* (unpubl.).

Zambonini, F. (1905): Über einige Mineralien von Canale Monterano in der Provinz Rom. *Z. Krist. Mineral.* **40**, 49-68.

Received June 1977, revised manuscript accepted January 1978.